

# Three-dimensional cellular architecture of the flagellar pocket and associated cytoskeleton in trypanosomes revealed by electron microscope tomography

Sylvain Lacomble<sup>1</sup>, Sue Vaughan<sup>1</sup>, Catarina Gadelha<sup>1</sup>, Mary K. Morphew<sup>2</sup>, Michael K. Shaw<sup>1</sup>, J. Richard McIntosh<sup>2</sup> and Keith Gull<sup>1,\*</sup>

<sup>1</sup>Sir William Dunn School of Pathology, University of Oxford, South Parks Road, Oxford OX1 3RE, UK

<sup>2</sup>Laboratory for 3-D Electron Microscopy of Cells, Department of Molecular, Cellular and Developmental Biology, University of Colorado, Boulder, CO 80309, USA

\*Author for correspondence (e-mail: keith.gull@path.ox.ac.uk)

Accepted 8 December 2008

Journal of Cell Science 122, 1081-1090 Published by The Company of Biologists 2009

doi:10.1242/jcs.045740

## Summary

This study uses electron tomography linked to a variety of other EM methods to provide an integrated view of the flagellar pocket and basal body area of the African trypanosome procyclic trypomastigote. We reveal the pocket as an asymmetric membranous ‘balloon’ with two boundary structures. One of these – the collar – defines the flagellum exit point. The other defines the entry point of the flagellum into the pocket and consists of both an internal transitional fibre array and an external membrane collarette. A novel set of nine radial fibres is described in the basal body proximal zone. The pocket asymmetry is invariably correlated with the position of the probasal body and Golgi. The neck region, just distal to the flagellum exit site, is a specialised area of membrane associated with the start of the flagellum attachment zone and signifies

the point where a special set of four microtubules, nucleated close to the basal bodies, joins the subpellicular array. The neck region is also associated with the single Golgi apparatus of the cell. The flagellar exit point interrupts the subpellicular microtubule array with discrete endings of microtubules at the posterior side. Overall, our studies reveal a highly organised, yet dynamic, area of cytoplasm and will be informative in understanding its function.

Supplementary material available online at  
<http://jcs.biologists.org/cgi/content/full/122/8/1081/DC1>

Key words: Trypanosome, Flagellum, Flagellar pocket, Basal body, Electron tomography, Golgi, Microtubule, Cytoskeleton, Secretion

## Introduction

Kinetoplast parasites are the aetiological agents for three severe but neglected diseases in developing countries: Leishmaniasis, Chagas’ disease and African trypanosomiasis. The parasites that cause all these diseases display variability of cell form during their life cycles, orchestrated by an internal cytoskeletal corset of microtubules that lies just beneath the plasma membrane (Gull, 1999). This microtubule array precludes vesicular transport to or from the plasma membrane. All such traffic is therefore focused on a critical structure: the flagellar pocket (Field and Carrington, 2004; Overath and Engstler, 2004). This pocket is a bulbous invagination of the plasma membrane that surrounds the site of flagellum exit from the cell body, an arrangement that is central to the success of these organisms as parasites. It allows the segregation of cellular and biochemical phenomena that enhance pathogenicity away from the exposed cell surface, concentrating them in a privileged ‘internal’ site (Gull, 2003).

The importance of the flagellar pocket is perhaps best exemplified in the African trypanosome, *Trypanosoma brucei*. This pathogen, spread by the tsetse fly, causes both a devastating human disease, African Sleeping Sickness and a similar disease, Nagana, of cattle. The flagellum of the trypomastigote form of *T. brucei* emerges from the flagellar pocket at the posterior end of the cell and is attached to the exterior of the cell along the length of the cell body. The *T. brucei* pocket provides the physical platform for plasma membrane domain differentiation. It is the normal cell surface site for localisation of receptors such as transferrin or CRAM (Field et al.,

2007; Hung et al., 2004; Steverding, 2000). It is the site of trafficking and recycling of glycosylphosphatidylinositol (GPI)-anchored surface proteins, such as procyclin (the major surface protein of the tsetse midgut form) and the variable surface glycoprotein (VSG) antigen (the major surface component in the mammalian bloodstream form). Finally, the flagellar pocket is also a key player in the trypanosome’s defence against attack by the innate and acquired immune systems (Allen et al., 2003; Chanez et al., 2006; Engstler et al., 2007; Field and Carrington, 2004; Hung et al., 2004; Landfear and Ignatushchenko, 2001; Overath and Engstler, 2004; Pays et al., 2006; Schwartz et al., 2005; Shiflett et al., 2007; Vanhollebeke et al., 2008). Flagellar pocket membrane dynamics are at their highest in the bloodstream form, but the general appearance and function of bloodstream and ‘procyclic’ cell (tsetse midgut form) pockets are similar.

Although the trypanosome flagellum is primarily a motility organelle, it and its associated parts perform many additional functions. The basal bodies help to position and segregate the kinetoplast (the mitochondrial genome) (Ogbadoyi et al., 2003; Robinson and Gull, 1991) and the flagellum itself is a sensory and signalling organelle (Oberholzer et al., 2007a; Oberholzer et al., 2007b). It also operates as an attachment organelle (Beattie and Gull, 1997; Vickerman, 1973). Finally, the trypanosome flagellum plays a key role in cell morphogenesis and cell division by defining the polarity of the cell and developmental axes (Broadhead et al., 2006; Ploubidou et al., 1999; Robinson et al., 1995). The single flagellum present at the start of the cell cycle is subtended from a

basal body, which has an associated probasal body that was formed in the previous cell cycle. This probasal body matures at the G1/S transition and forms a new flagellum (Sherwin and Gull, 1989a). The new flagellum tip attaches to the lateral aspect of the old flagellum through a mobile transmembrane junction – the flagella connector – that acts as a cytotoxic element influencing the morphogenesis and construction of the cytoskeleton and structure of the nascent daughter cells (Briggs et al., 2004; Moreira-Leite et al., 2001). During this process, the internal cytoskeleton of the trypanosome is restructured, and a new flagellum attachment zone (FAZ) filament structure and associated microtubule quartet develop to accommodate the new flagellum. In effect the FAZ forms a seam in the subpellicular corset of microtubules that provides shape, polarity and form for the trypanosome cell body (Vaughan et al., 2008).

Recent work has led to an increased understanding of the importance of the flagellar pocket, its biochemistry and cell biology, yet we lack a clear understanding of its detailed architecture; in particular, how the membrane systems relate to the underlying cytoskeletal architecture. This is particularly unfortunate as RNAi analyses in *T. brucei* are providing mutant phenotypes with dramatic changes in flagellar pocket structure and operation (Allen et al., 2003; Bonhivers et al., 2008; Broadhead et al., 2006; Chanez et al., 2006; Garcia-Salcedo et al., 2004). Precise understanding of these phenotypes is hampered by the lack of detailed understanding of the normal flagellar pocket. We have now addressed this lack of knowledge and other issues using more reliable and better resolution structural studies. In a more general cell biology context, the highly structured trypanosome flagellar pocket provides us with an opportunity to study fundamental issues of how orchestration of membrane and cytoskeletal interactions produces defined areas of differentiated eukaryotic cell surface.

## Results

### Flagellar pocket architecture in procyclic trypanosomes

To preserve the architecture of the flagellar pocket, procyclic trypanosomes from log-phase were fixed by the addition of glutaraldehyde directly to the culture medium, thereby increasing the rate of fixation of the dynamic membrane system and minimizing the chances of osmotic artefact. To characterise these well-preserved pockets, much of the flagellar pocket and the surrounding cytoplasm were reconstructed in 3D by electron tomography, as described in the Materials and Methods. We selected, modelled and analysed flagellar pockets from cells, and then tested all observations from these tomograms in an iterative manner, using a library of over a thousand thin section electron micrographs. Opinions from all this sectioned material were then tested with images obtained from negatively stained whole mounts of detergent extracted cytoskeletons.

Here, we present conclusions integrated from all these preparations to describe the basic architecture of a flagellar pocket. We have used data from a number of tomograms, but individual pocket organisation is most obviously revealed by examination of a particular tomogram that includes ~80% of the volume from the anterior flagellar pocket associated with the new flagellum of a very late stage dividing cell, immediately prior to cytokinesis. This model therefore represents flagellar pocket architecture at its initial state in the cell cycle, illustrating standard pocket features. Fig. 1 shows a model generated from a tomographic reconstruction of this cell (referred to hereafter as tomo 1). Tomo 1 is derived from three adjacent serial 250 nm sections that yielded 435 tomographic slices

of ~1.6 nm (as illustrated in Fig. 1B-D); these encompass ~2  $\mu\text{m}^3$  of the cell. Fig. 1A represents this serial tomogram diagrammatically. Fig. 1B displays a slice at the level where the flagellum is emerging from the pocket area, Fig. 1C is a slice at the level of the basal body and probasal body, and Fig. 1D is a slice from a lower region of the pocket; it also reveals the kinetoplast within the mitochondrion. Movie 1 displays this reconstructed volume and shows the invagination of the plasma membrane that forms the flagellar pocket, with the single flagellum emerging from the flagellar pocket and onto the cell surface.

A scanning electron micrograph (Fig. 2A) illustrates the general volume of the tomogram and how the flagellum exits the cell surface at the posterior end of the cell. A view of the model (which is presented fully in Movie 1) is seen in Fig. 2B. Each structure in the model has a particular colour code, which is detailed in Table S1 (see supplementary material). Tomo 1 and the model constructed from it illustrate most of the organelles/structures present in this area of the cell. Fig. 2B shows a view restricted to the important cytoskeletal and membrane structures directly associated with the flagellar pocket area. The kinetoplast (a specialised region containing the mitochondrial DNA) is located at the proximal end of both basal body and probasal body. Cytoskeletal components, such as flagellum attachment zone filament, microtubule quartet and collar, in addition to Golgi apparatus and endoplasmic reticulum, are also included in this tomogram and model.

We next defined an origin and a set of Cartesian axes in order to compare positions, orientations and the architecture of components. The centre of the proximal end of the basal body is a singularity in the cell that allows the definition of an origin, and we used the position and orientation of two specific components to define the axes (Fig. 2C). The *z*-axis is the principal axis of the axoneme; the *x*-axis lies in the plane of the central pair microtubules at the point where they are nucleated; the *y*-axis points towards the associated probasal body, and positive *x* is chosen so the coordinate system is right-handed (Fig. 2C,D). These axes define four quadrants to which we can ascribe both position and orientation of the major pocket structures. Moreover, they facilitate the orientation, and therefore comparison, of comparative tomograms.

The basal body defines the proximal end of the flagellum, and the axoneme that extends from it invades the flagellar pocket asymmetrically (Fig. 2B,D). The basal body is represented by an extreme proximal end set of microtubule triplets followed by the more distal doublet microtubule transition zone and then a basal plate (from which the central pair of singlet microtubules extends). After this, the 9+2 canonical microtubule axoneme extends up to the site where the flagellum exits the flagellar pocket. At this point, the axoneme is joined by the paraflagellar rod (PFR), a unique lattice-like structure situated alongside the axoneme (Fig. 2B). A newly formed probasal body, containing triplet microtubules, lies close to and parallel with the basal body (Fig. 2B,D). In addition, a set of four specialised microtubules, termed the microtubule quartet (Taylor and Godfrey, 1969), is nucleated between the basal body and probasal body and runs along, up and around the flagellar pocket membrane in a left-handed helical pattern, finally inserting into the subpellicular array of microtubules (Fig. 2B,D). The microtubule quartet traverses the flagellar pocket collar, an electron-dense structure that defines an annulus at the neck of the flagellar pocket (Fig. 2B).

There is an extensive network of endoplasmic reticulum and a single Golgi apparatus located within the vicinity of the flagellar pocket (Fig. 2B). Comparisons between tomo 1 and other

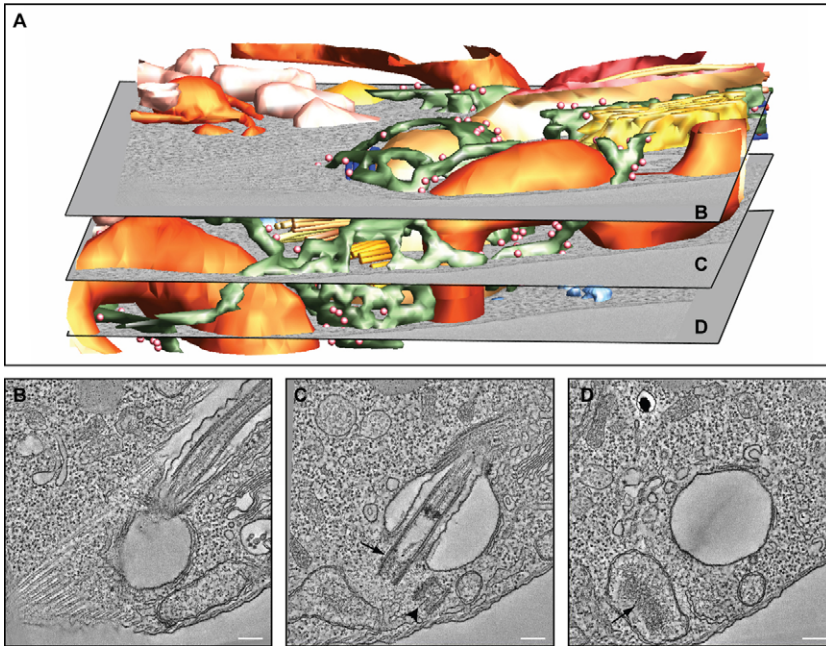


**Fig. 1.** Tomographic representation. (A) Surface rendering representation of tomo 1, colours were subjectively attributed to organelles and structures around the flagellar pocket area (supplementary material Table S1). (B-D) Individual (sequential but not adjacent) tomographic slices (~1.6 nm thick) extracted from the 435 slices that comprise the reconstructed 3D volume of tomo 1. (B) A slice of the actual tomogram at the level where the flagellum emerges from the flagellar pocket. (C) A slice at the level of the basal body (arrow) and probasal body (arrowhead). (D) A slice at the lower region of the pocket also showing the kinetoplast (arrow) within the mitochondrion. Scale bars: 200 nm in B-D. Movie 1 (supplementary material) shows the original tomographic reconstruction coupled with the segmentation model.

tomograms and thin sections from cells in corresponding stages of the cell cycle reveal that these architectural features and positions are consistent, reflecting the high fidelity of cellular organisation.

#### Flagellar pocket boundaries

Tomo 1 and many images of conventional thin sections show that the flagellum invades the flagellar pocket asymmetrically. This arrangement results in a bulge on one side of the flagellar pocket in quadrants 1 and 2 (Fig. 2D). Both the probasal body and Golgi are invariably located to the bulge side of the flagellar pocket (Fig. 2B,D; Fig. 3A).

Two boundaries define the flagellar pocket and allow the differentiation of the flagellar pocket membrane as distinct from the other two main types of surface membranes in this cell: the external surface plasma membrane and the flagellar membrane. Surrounding the transition zone of the basal body there is a boundary that defines the entry point of the flagellum at the pocket base. Where the flagellum emerges to the cell exterior, there is an 'exit point', which defines the top of the pocket (Fig. 3C). These two boundary zones are structured such that there is intimate connection between the membrane and the underlying cytoskeleton. The flagellar pocket exit boundary is defined by two elements: an electron-dense structure termed the collar and the neck region (Henley et al., 1978; Sherwin and Gull, 1989a) (Fig. 3B). The collar (Fig. 3D,F) surrounds the exit boundary zone on the cytoplasmic face of the flagellar pocket membrane. At this point, the flagellar pocket membrane is constricted and closely aligned with the inner sleeve of the flagellar membrane (Fig. 3D,F). Given its amorphous electron density, this material is difficult to model, but our careful assessment of different tomograms and many thin sections suggests that there is some variability in the distribution of this material at the point that it is traversed by the microtubule quartet (Fig. 3G,H). Obviously, the collar must be traversed at some point by the microtubule quartet (which is always tightly attached to the inner face of the pocket membrane), which suggests some regional dislocation in the collar components. A difficulty is that in such amorphous electron-dense structures it is impossible to discern

subregions of distinct biochemical components. However, detergent- and salt-treated isolated flagella do show a very discrete annulus of collar material (Fig. 4H), suggesting there may be a central collar annulus and more loosely associated components that contribute to the electron density.

Figs 3I,J illustrate the flagellar pocket exit point where the flagellum leaves the cell body and lies on the external cell surface. Here, we can observe a specific plasma membrane region immediately outside the pocket that has previously been termed the neck region (Henley et al., 1978). The neck region has a cylindrical form and a diameter only slightly larger than the flagellum itself. This neck region membrane area defines a transition between the flagellar pocket internal balloon membrane (which is delineated by the collar) and the external plasma membrane of the overall cell surface (Fig. 3I,J). The neck region, like the flagellar pocket, is therefore a distinct region of the plasma membrane. The main group of subpellicular microtubules does not invade this neck region (Fig. 3J) but bypasses it at a higher level in the cell under the main plasma membrane region. However, our tomography shows that the microtubule quartet occupies this neck region membrane after traversing the collar and before emerging to join the major subpellicular array (Fig. 5A,C). We note that we can often define a single microtubule (seen in the view of the model of tomo 1 in Fig. 5A,C and marked as 'the neck microtubule') that lies alongside the FAZ filament structure on the opposite side to the microtubule quartet. Both ends of this microtubule are visible within the volume of tomo1. Alongside the microtubule quartet, the start of FAZ filament components can also be defined in this neck region (a FAZ fibre and the cytoplasmic part of the macula adherens) (Fig. 5A). The FAZ is composed of the microtubule quartet and associated membrane, together with a specific FAZ filament structure on the right-hand side of the quartet (when viewed towards the anterior end of the cell). There are also membrane-membrane macula adherens connections between the plasma membrane and flagellar membrane in the region over the FAZ filament (Fig. 5B). However, the linkage between cell body and flagellar membrane appears to be made only after the point of true exit of the flagellum from the

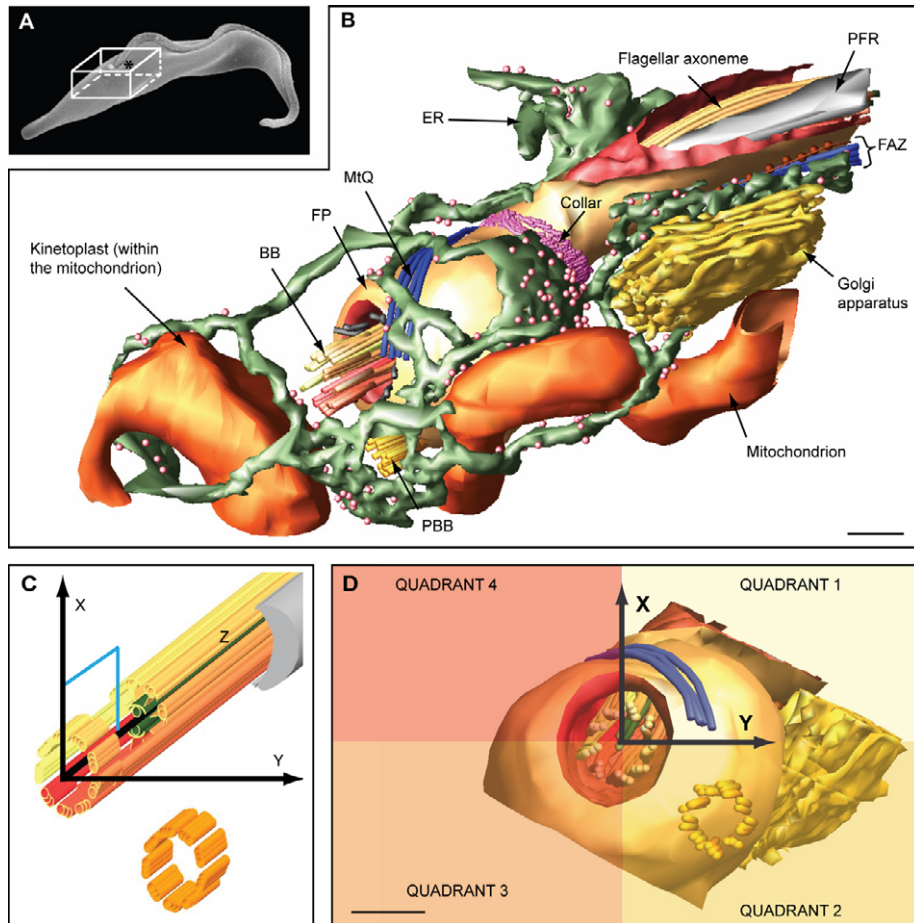


**Fig. 2.** Flagellar pocket architecture.

(A) Scanning electron micrograph illustrates the position of the flagellar pocket region. The flagellum exit point on the cell surface is labelled with an asterisk. (B) 3D model illustrates the relationship of the cytoskeletal and membrane structures associated with the pocket. Abbreviations: BB, basal body; PBB, probasal body; FP, flagellar pocket; PFR, paraflagellar rod; MtQ, microtubule quartet; FAZ, flagellum attachment zone; ER, endoplasmic reticulum. (C) This cartoon defines the axes that we used to position tomograms. The origin point is defined by the centre of the basal body at its most proximal end. The z-axis runs up the length of the axoneme; the x-axis is defined by the plane of the central pair microtubules at the point at which they are nucleated; finally, the y-axis points towards the probasal body. (D) A model of tomo 1 with many of the components excluded has been orientated such that the view is along the z-axis. This allows the definition of four quadrants in the cell useful for positioning organelles and structures and comparison of tomograms. Scale bars: 200 nm.

cell at the place where the PFR begins, so providing the internal architecture of the flagellum necessary for cytoskeletal connections. Thus, the neck region defines a fourth specific region of surface membrane within the trypanosome cell.

We now turn to the basal flagellar entry boundary zone, where we can define at least three structural features that appear to have important roles in separating the flagellar pocket membrane from the flagellar membrane. These structures are the internal transitional fibres, the radial fibres and the external collarette (Fig. 3B,E; Fig. 4A-C). The transitional fibre array radiates from the distal end of the basal body microtubule triplets and connects with the flagellar membrane at the base of flagellar pocket (Fig. 4A). The second element is located on the outside of the flagellar membrane in the lumen of the flagellar pocket; it is termed the collarette (Fig. 3E; Fig. 4B). This decorates the external surface of the flagellar membrane surrounding a region of the transition zone of the basal body. This was originally described in longitudinal section (Vickerman, 1973; Vickerman and Tetley, 1990), but we now show that the collarette has an elaborate structure in transverse sections, including nine regularly spaced double-tube-like units (Fig. 4B, black arrows). These are connected to each other by plate-like fibrillar structures on the flagellar membrane (Fig. 4B, white arrows). In addition to these two features, EM tomography has highlighted a previously unrecognised set of structures, which we term 'radial fibres' lying inside the flagellar membrane (Fig. 3B; Fig. 4C,D) and alongside the basal body proximal region. These fibres are  $6 \pm 1.6$  nm in diameter and  $280 \pm 20$  nm in length, and make a discrete inflection at the point where they enter the

flagellum (Fig. 4C,D). The ninefold radial symmetry of the transitional fibres, collarette and radial fibres mirrors the radial symmetry of the doublet microtubules of the basal body transition zone, emphasising a discrete transmembrane influence from the internal cytoskeleton to external membrane adornments.

#### Setting the FAZ architecture

The positions of the axoneme and PFR relative to the FAZ filament structure and microtubule quartet are precisely defined (Fig. 5B). The FAZ comprises a set of structures on either side of the flagellar/plasma membrane that forms a discrete seam in the subpellicular corset of microtubules linking the cell body to the flagellum. Importantly, our previous work has shown that the quartet microtubules are anti-parallel to the rest of the microtubules of the subpellicular array in having their plus ends at the anterior of the cell (Robinson et al., 1995). The PFR has been well described and is known to be connected to the axoneme via doublets 4-7 (Fig. 5B).

Electron tomography revealed the 3D positioning between the axoneme, FAZ and PFR within the flagellar pocket area. Using the previously defined axes, the microtubule quartet is nucleated in positive quadrant 1 and follows a left-handed helical path through to quadrant 4 and back around to quadrant 1 (Fig. 2D; Fig. 5A). During this transit, the microtubule quartet is firmly attached to the flagellar pocket membrane (Fig. 3B,G). Three other specific points about the microtubule quartet can be noted: they are associated with electron-dense material, until they reach the neck region there is no accompanying FAZ filament structure. Finally, they are tightly

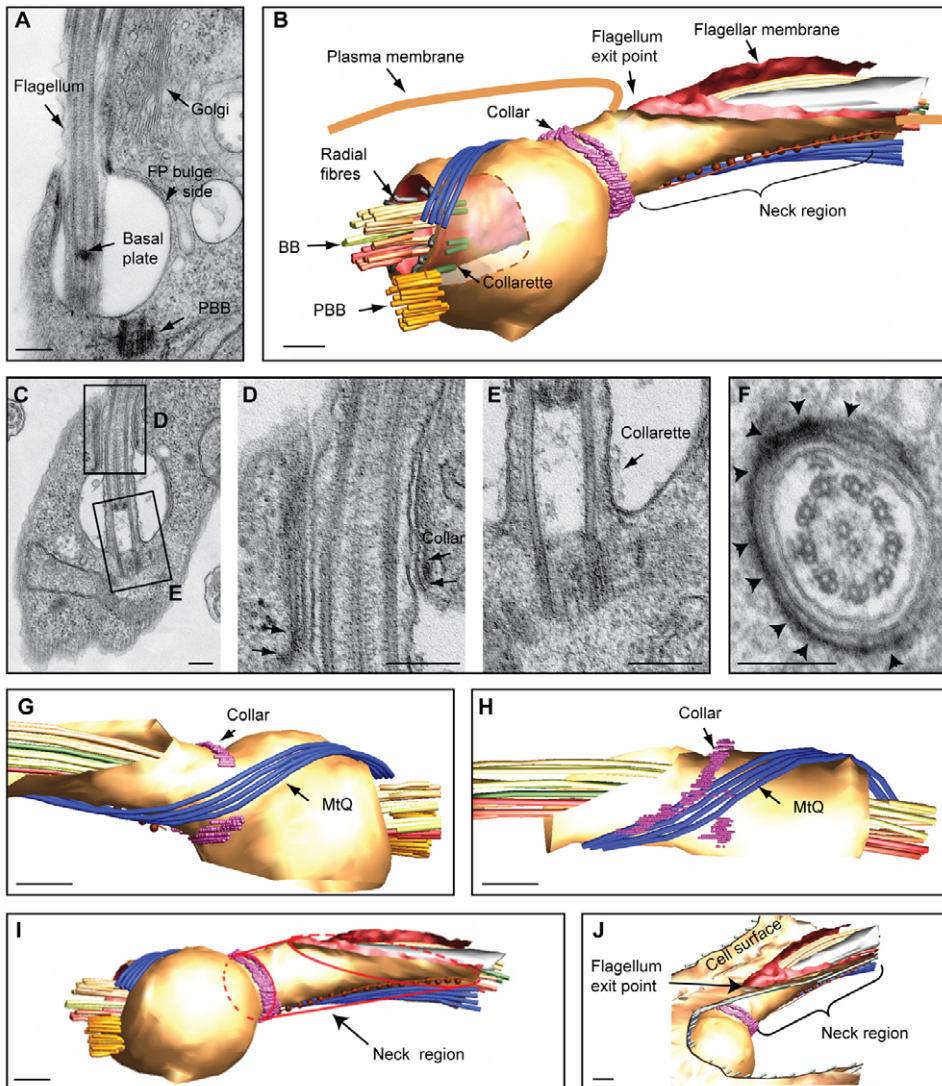


**Fig. 3.** Flagellar pocket boundaries. (A) Representative thin-section electron micrograph illustrating the asymmetry of the flagellar pocket (FP) volume. Note the bulge side towards the cell interior accompanied by the probasal body (PBB). Note also a line of symmetry between the PBB and the single Golgi stack. (B) Model of tomo 1 showing only major membrane and cytoskeletal areas. Two boundaries define the flagellar pocket: the collar and the neck region defining the exit boundary, the radial fibres and collarette defining the flagellum entry boundary. BB, basal body. (C) Representative thin-section electron micrograph illustrating the boundaries that outline the flagellar pocket. Rectangles outline the exit and entry boundaries shown at higher magnification in D and E, respectively. (F) Representative cross-section depicting the electron-dense collar (arrowheads) on the cytoplasmic side of the neck region membrane. (G,H) Views of collar density modelled from two tomograms showing a level of variation. The graphical representation of the collar shown here corresponds to the general electron-density patterns (arrowheads) seen in F. MtQ, microtubule quartet. (I) A view of the model of tomo 1 to illustrate the vase-like neck region through which the flagellum finally emerges from the cell. (J) Another view of the tomogram model to illustrate the neck region and flagellum exit point with a region of the cell surface membrane and associated subpellicular microtubules in place. Scale bars: 200 nm.

adjacent with essentially no inter-microtubule gaps, whereas when they are incorporated into the subpellicular array the intermicrotubule distance is a noticeable  $31 \pm 5$  nm. The FAZ filament structure is not present on the flagellar pocket membrane and appears only distal to the collar on the neck region. In this region the FAZ filament structure follows the final part of the same helical path as the microtubule quartet (Fig. 5A,C)

Tomo 1 illustrates that the spatial positioning of the axonemal doublets is invariant from their proximal ends to the main axoneme with the collocated PFR, such that there is no twisting of the axoneme between the basal body and the start of the PFR. Thus, the FAZ has to follow their precise left-handed helical path to be inserted into the subpellicular microtubule array at a specific position, which is essential for them to connect with this invariant internal axonemal organisation. Fig. 5C illustrates this insertion of the microtubule quartet and FAZ filament structure between two subpellicular microtubules, thus setting up this invariant positioning and discrete seam in the subpellicular corset of microtubules (Fig. 5B).

#### Subpellicular microtubule corset

The microtubules of the subpellicular corset are highly ordered in a linear, planar, array, showing a regular intermicrotubule spacing

of  $24 \pm 5$  nm and  $23 \pm 5$  nm microtubule to plasma membrane. Each microtubule is crosslinked to its neighbours and to the plasma membrane by specific linkers. The inter-microtubule spacing is invariant along the cell, even though the cell diameter varies. Thus, microtubules must be of different lengths with stops and starts along the cell body. When one subpellicular microtubule ends (either the plus or minus end), those on either side continue and then become crosslinked to each other. More than 50 subpellicular microtubules are present in the cell volume encompassed in tomo 1. Fig. 5D models a region of the subpellicular corset: one end of five microtubules and both ends of two lie within the tomogram (all ends are annotated with either a hash symbol or an arrow). The subpellicular microtubules appeared to end preferentially at points of decreasing cell diameter or when the plasma membrane bends/folds. All subpellicular microtubules (except the microtubule quartet) are oriented so their plus ends face the posterior end of the cell (Robinson et al., 1995). Fig. 5E illustrates the ending of two microtubules, showing the subsequent approach of the neighbouring lateral microtubules. A triangle of clear space to the point where both lateral microtubules have come together and possess the normal inter-microtubule distance is apparent on these tomographic slices.

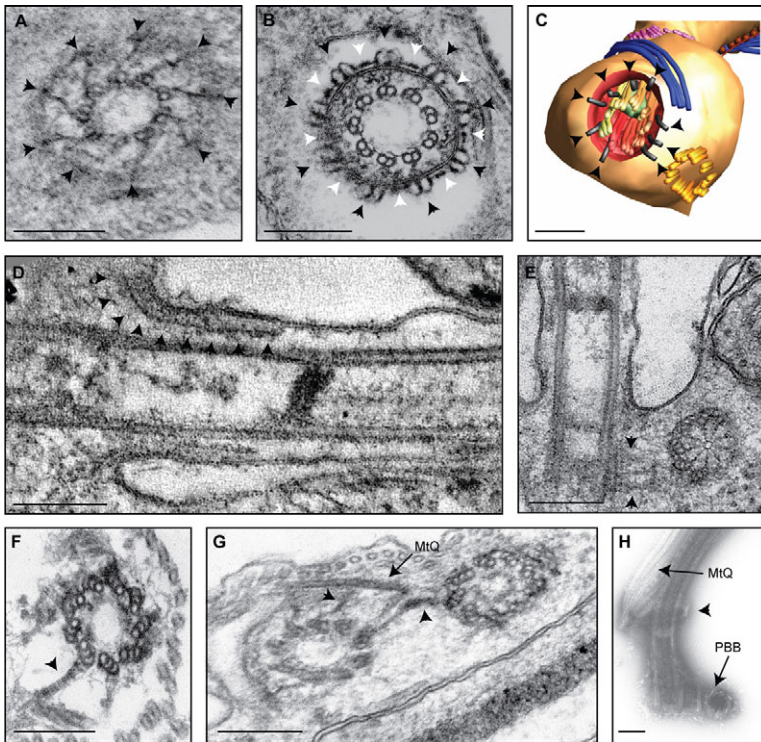


**Fig. 4.** Basal bodies and flagellum entry boundary.

(A) Representative cross-section of the transitional fibres radiating out from the basal body doublet microtubule region. (B) Representative cross-section of the collaette surrounding the flagellar membrane base. Black arrowheads denote the double tubular structures opposite each microtubule doublet. White arrowheads denote the linking fibrous sheath connecting these double tubular structures. (C) A model of tomo 1 showing the position of the radial fibres (arrowheads) located between the basal body and the surrounding membrane. (D) The sum of five individual tomographic slices (corresponding to a thickness of 8.5 nm) from a tomogram, illustrating the structure of a single radial fibre (arrowheads). (E) Thin section illustrating the cartwheel of the probasal body and striated fibre connections between probasal body and basal body (arrowheads). (F) Thin section of a 9+0 triplet microtubule basal body, illustrating a striated fibre extending from a C-tubule (arrowhead). (G) Thin section of a basal body and probasal body illustrating connections between each other and the microtubule quartet (MtQ) (arrowheads). (H) Electron micrograph of a detergent-extracted, salt-treated and negatively stained preparation of an isolated flagellum complex. Striated fibres have maintained the connections between the probasal body, basal body and microtubule quartet. Also seen in this micrograph are the microtubule quartet and the collar central annulus (arrowhead). PBB, probasal body. Scale bars: 200 nm.

We then addressed how this interlinked microtubule corset is modified to allow the exit of the flagellum from the cell body. A number of general points can be illustrated by the specific arrangement of subpellicular microtubules in Tomo 1. First, a specific set of microtubules end at the posterior side of the flagellum exit point and neck region. In fact, three microtubules end close together at this point, and significantly this is the only position where we have observed two adjacent microtubules ending together. Moreover, the ending of three microtubules in this position opens up a space for the exit of the flagellum through the microtubule corset (Fig. 5D, arrowheads). Importantly, we note that two of these microtubules are short and their plus and minus ends are both included in the volume of the tomogram (highlighted in Fig. 5D). Other microtubules then border the space left by these microtubule ends and form a lateral boundary at the corset as they move around the flagellar pocket exit point. We note that, because of the insertion of the FAZ filament structure and microtubule quartet into the array at the anterior cell side of the flagellum exit point, very few subpellicular microtubules are required to end on this side of the flagellum exit point (Fig. 5C,D).

#### Basal body – probasal body organisation

The proximal end of the basal body is positioned in the cytoplasm as a 9+0 triplet arrangement of microtubules, but a 9+0 arrangement of doublet microtubules is found in the transition zone that intrudes into the flagellar pocket (Fig. 4E; Fig. 5A). Subsequently, the central pair is nucleated, forming the canonical 9+2 axoneme. A probasal body is positioned in the cytoplasm on the bulge side of the flagellar pocket within quadrant 2 (Fig. 2D; Fig. 3A; Fig. 4E); it is composed of 9 + 0 triplet microtubules.

The basal body and probasal body are physically connected, and both are connected to the kinetoplast. The latter connection is mediated by the Tripartite Attachment Complex (Ogbadoyi et al.,

2003), which is not dealt with here. The connections between basal body and probasal body are so strong that they allow co-isolation of the two structures in flagellum preparations (Fig. 4H). In thin sections, we observed fibres leading from the basal body and additional connections between the probasal body and the microtubule quartet (Fig. 4E,F,G). Our view of these structures is a composite achieved by integrating information from all three of our imaging techniques. Different levels of substructure resolution are achievable with each technique. Integrating information from all methods reveals that the connections include two sets of striated fibres on the basal body. The first set consists of two striated fibres that lead from the C-tubule of triplet microtubule number 5 and connect with the microtubule quartet. The second set includes three striated fibres leading from the C-tubule of triplet microtubule 6. The most distal one connects with the microtubule quartet, and filaments lead from this connection to the probasal body. The other striated fibres on microtubule 6 do not connect to the microtubule quartet, but they connect to the probasal body via a set of filaments. Fig. 4F,G illustrates some of these connections.

#### Secretory system organelles

The crucial feature of cytoskeletal organisation and flagellar exit from the trypanosome cell is that it provides the framework for the discrete membrane environment of the flagellar pocket. This pocket is not only an area of differentiated surface membrane (albeit internal to the cell), it also provides a focus for a highly organised secretory and endocytic system. Our tomography revealed that a prominent feature of this secretory system is a system of branching tubules and flattened sacs that comprises a section of endoplasmic reticulum (ER). The ER in the vicinity of the flagellar pocket has both fenestrated and sheet-like sections. A specific sheet of ER is located over the bulge side of the flagellar pocket in quadrant 1 (Fig. 2B; Fig. 6A). Noticeably, this flat sheet does not extend onto the flagellar

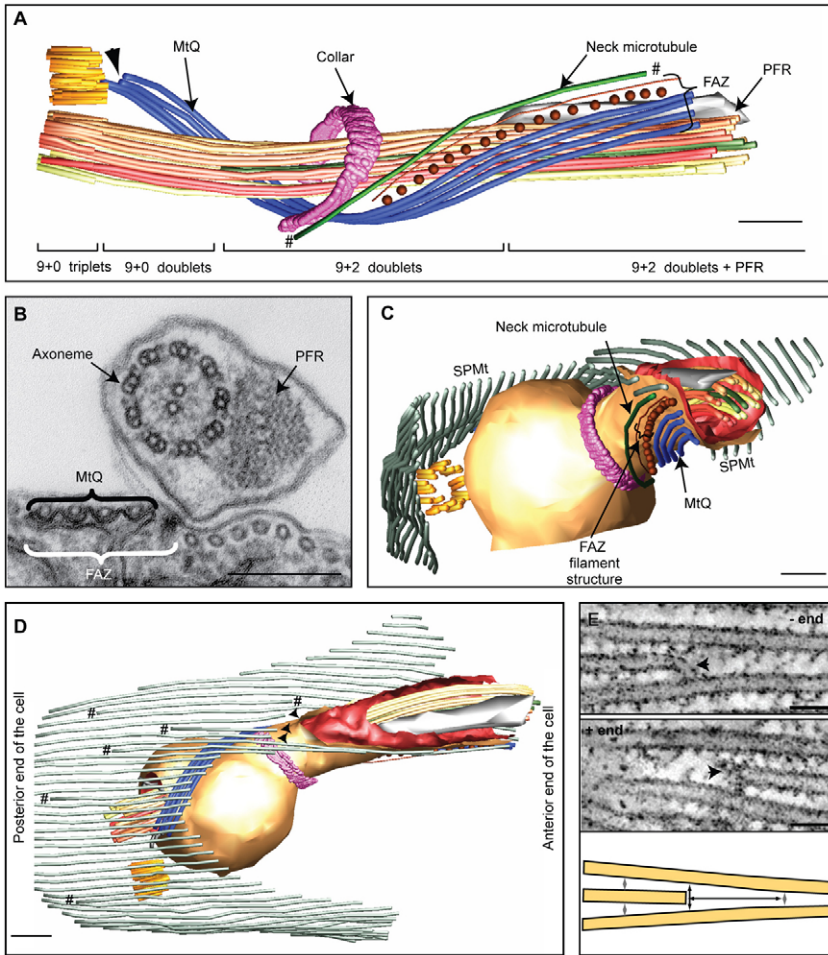


**Fig. 5.** Cytoskeletal structure. (A) Tomo 1 model view in which all membrane objects were excluded in order to emphasise the cytoskeletal elements around the flagellar pocket. Note the left-handed helical pattern of the microtubule quartet (MtQ), the position of the collar relative to the axoneme and the origin points of the flagellum attachment zone (FAZ) filament structure and paraflagellar rod (PFR). The origin of the microtubule quartet is indicated by an arrowhead. Scale bar: 200 nm. # indicates where both ends of the neck microtubule can be seen within the tomogram volume. (B) Representative cross-section of the flagellum (post-exit point) and its association to the cell body. The microtubule quartet (MtQ) and associated ER are seen to the left of the FAZ filament structure (when viewed from the posterior end of the cell). Scale bar: 200 nm. (C) Tomo 1 model view (observed from the anterior end of the cell) showing the MtQ and the FAZ filament structure on the neck region membrane. These structures then join the subpellicular microtubule array (SPMt). A neck microtubule is present on the neck region membrane on the other side of the FAZ filament structure. Scale bar: 200 nm. (D) General view of the subpellicular microtubule array within the tomographic volume of tomo 1. Microtubule ends within the tomographic volume are marked with # or an arrowhead. Plus ends of microtubules will be at the posterior end of the cell (left-hand side of this image). The arrowheads define the ending of three microtubules that open up the space required for the exit of the flagellum. Plus and minus ends of some subpellicular microtubules in which both ends could be seen are enlarged in E. Scale bar: 200 nm. (E) The tomographic volume of tomo 1 was rotated and sliced in order to bring the image of two microtubule ends into view (arrowheads). Plus and minus endings of the microtubules leave an enhanced gap between the microtubules for a short distance as illustrated. Note also the regularly arranged cross bridges between microtubules. Scale bars: 50 nm

pocket area in quadrant 4 of tomo 1 (Fig. 6B). A region of the ER is organised into fenestrated mesh-like membranes that eventually run parallel to the cis side of the Golgi apparatus (Fig. 6A,C). The Golgi itself is invariably positioned close to the bulge side of the flagellar pocket (Fig. 2B; Fig. 3A; Fig. 6C), with a discrete cis/trans orientation. Different orientations of the tomo 1 model illustrate different views of the ER and Golgi network and their relationship to cytoskeletal structures (Fig. 6A–D), and the asymmetry of the flagellar pocket. Examination of Fig. 6 and Movie 1 reveals that the Golgi is positioned adjacent to the neck region of the flagellar pocket and is associated with the discrete area of the FAZ filament and microtubule quartet on this neck membrane.

## Discussion

Trypanosome ultrastructure has been studied using electron microscopy for over 50 years. This portfolio of work on many different types of trypanosomes has led to a deep understanding of cellular components. However, with few exceptions, there has been little progress in integrating the descriptions of individual components into a holistic view of this very highly ordered cell. This study uses electron tomography linked to a variety of other EM approaches to provide the first integrated view of the flagellar pocket and basal body area of this cell. The vase-like pocket is a central feature of the cell biology and pathogenicity of trypanosomes. The 3D flagellar pocket architecture described here provides new insight allowing deeper understanding of the

phenotypes of RNAi mutants where the flagellar pocket either disappears (Bonhivers et al., 2008) or increases in size (Allen et al., 2003; Broadhead et al., 2006; Garcia-Salcedo et al., 2004).

The use of tomography revealed the important feature of flagellar pocket asymmetry, showing very clearly the bulge on the probasal body side. This is the side adjacent to the main volume of cytoplasm and the area where the Golgi apparatus is located. There are obvious structural advantages to this asymmetry for membrane traffic but it is unclear whether it occurs as a consequence of increased membrane activity at that the bulge face or is imposed by the adjacent cytoskeletal structures. There are clear candidates for the latter phenomenon in the positioning of the probasal body and the microtubule quartet. Both of these could either influence or impose the asymmetry. In procyclic forms we have consistently seen that this bulge pocket membrane in quadrants 1 and 2 is covered on its cytoplasmic side by a plate-like sheet of endoplasmic reticulum. The ER of the trypanosome is known from light microscope imaging of components such as BiP to form a highly branched tubular network throughout the cell (Bangs et al., 1993). However, the tomograms reveal both plate-like and fenestrated areas. A particular fenestrated sheet is associated with the cis-Golgi.

*T. brucei* possesses a single Golgi apparatus that has a very particular location influenced by a specific centrin-containing structure described at the light microscope level. Warren and co-workers have shown that the new Golgi appears de novo adjacent to the old and develops over around 2 hours. The location of the

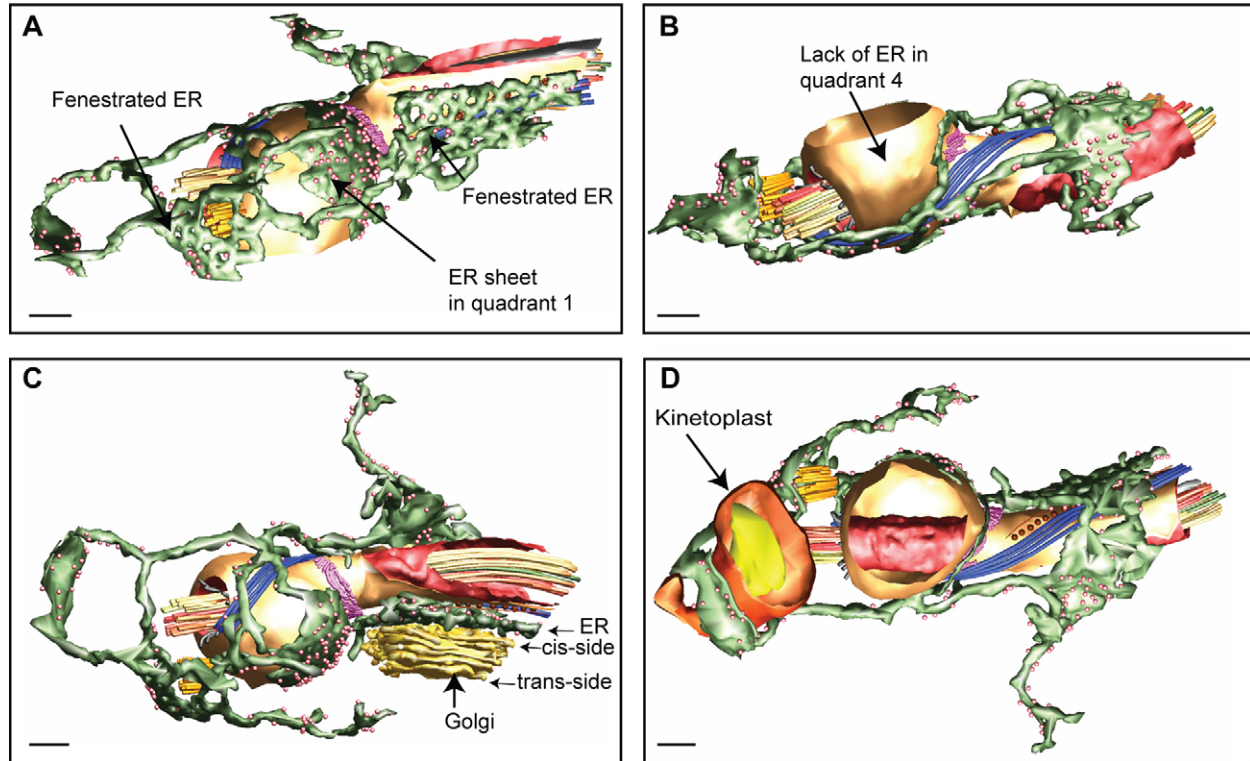


**Fig. 6.** ER, Golgi and kinetoplast. These model views were chosen from the surface rendered representation of tomo 1 to provide a 3D impression of the complex endoplasmic reticulum (ER) architecture around the flagellar pocket. (A) A region of ER forms a sheet, closely adjacent to and covering the flagellar pocket membrane, that is continuous with an area of fenestration. (B) The model view in A was tilted 180° to show here the absence of ER lamina on the opposite side of the flagellar pocket. (C) The model view in A was tilted ~90° around the z-axis to show here the Golgi localization relative to the ER and neck region: the single Golgi stack is adjacent to the fenestrated region of ER, following the line of symmetry with the probasal body and the bulge side of the flagellar pocket (see also Fig. 2A). The pink spheres represent individual ribosomes. (D) The kinetoplast region of the mitochondrion is illustrated in this model view. Scale bars: 200 nm.

new Golgi is determined by the position of the new basal body complex (He et al., 2004). Particular centrins locate to both the basal body and an additional bilobed structure near to the Golgi apparatus. One lobe is associated with the old Golgi, and the other is associated with the forming Golgi. In RNAi knock-down experiments, depletion of TbCentrin1 inhibited duplication of the basal body, whereas depletion of TbCentrin2 also inhibited duplication of the Golgi (He et al., 2005). Moreover, duplication of the bilobed structure is dependent on the single polo-like kinase (PLK) of *T. brucei* (TbPLK). Depletion of TbPLK leads to abnormal bilobed structures and concomitant inhibition of normal Golgi structures. These and other data suggest that the bilobed structure may be a primary scaffold for assembly of the new Golgi (de Graffenried et al., 2008). We were unable to discern a specific separate cytoskeletal structure in this area. However, our 3D description suggests that the neck region is a good candidate for a cytoskeletal structure that defines the position of the single Golgi.

The definition of this discrete neck region of the pocket comes from specific observations using tomography. We, and others, have long believed that the flagellum in trypanosomes facilitates the differentiation of three different areas of surface membrane – the cell surface plasma membrane, the flagellum membrane and the flagellar pocket membrane. Not only can these be defined structurally, but they have distinct biochemical properties and functions. The neck region now has to be added as a fourth surface membrane domain. It is on this domain that the FAZ filament is initiated and the quartet of microtubules associates with the filament

after its traverse around the flagellar pocket. In essence, the neck region represents a post collar/pre-flagellar exit point domain.

The electron dense collar forms an annulus around the top of the flagellar pocket. Clues to the identity of collar components have recently come from the identification of the protein Bilbo1 (Bonhivers et al., 2008) and from our laboratory in the identification of proteins with specific membrane interacting domains (Neil Portman and K.G., unpublished). The collar provides a clear separation between the flagellar pocket and the neck region membrane and, although present on the cytoplasmic face of the membrane, may well participate in the selective retention of surface receptors in the flagellar pocket. Obviously, the cytoskeletal architecture of the collar provides a fundamental mechanism for defining a fenestration in the subpellicular array of microtubules and an annulus whereby the surface plasma membrane can fold over and into the pocket. Moreover, the collar may operate as a cytoplasmic valve that regulates the entry and exit of material into the pocket lumen, which is known to be a privileged site for glycoconjugates (Atrih et al., 2005).

The base of the pocket is defined by another complex that interlinks the membrane with the underlying cytoskeleton, but this time it is the cytoskeletal structures of the flagellum that interact with the pocket base. One of these is the direct linkage of the transitional fibres from the basal body to the membrane. These nine transitional fibres are an integral part of many flagella and ciliary systems (Geimer and Melkonian, 2004; O'Toole et al., 2003). In addition, the trypanosome flagellum membrane base exhibits the

collar, originally described in longitudinal section by Vickerman (Vickerman, 1973) and now revealed as a particularly structured adornment on the external flagellar membrane base. Although we have no information on components or precise function for the collar, it appears well designed to act as an external sleeve, allowing membrane to be constrained and formed into the tube required to encase the flagellar axoneme. The membrane does not have any significant curvature until it reaches the very base of the collar, at which point it immediately flares out to form the base of the pocket. Our tomography and thin section analysis has revealed a novel internal structure – the radial fibres – which again reflects the ninefold symmetry of the basal body.

The radial fibres appear to provide another basal buttress and are characterised by a short segment that then kinks into a longer distal segment lying alongside the microtubules of the basal body under the initial region of the flagellum membrane. These distal regions of the radial fibres invade the flagellum for about half the length of the transition zone and are an internal reflection of the external collar. The radial fibres are associated only with the basal body and not the probasal body, and hence appear to be associated with maturation and docking with the membrane. One might confuse these structures with intraflagellar transport (IFT) particles (Bastin et al., 2000) but comparisons reveal that these latter structures are of variable length and are generally seen further up in the flagellum. Moreover, the radial fibres are present in fully elongated flagella and have a consistent ninefold symmetry that IFT particles do not. However, it is possible that the role of these radial fibres also encompasses roles in providing the physical base for docking and assembly sites for flagellar components (Rosenbaum and Witman, 2002; Stephan et al., 2007).

Trypanosome basal bodies perfectly exhibit the binary inheritance pattern that has been maintained throughout much of evolution for both centrioles and basal body complexes. The probasal body is always positioned at a specific location in the cell close to the basal body; specific sets of striated fibres link the two and make connections to the microtubule quartet that can be viewed as a specific example of a microtubule rootlet that is so characteristic of highly organised protistan cells (Moestrup, 2000). This microtubule quartet is a key feature of the trypanosome cell. The tomographic reconstructions now reveal its nucleation between the basal body and probasal body, its extended traverse around the pocket crossing the collar, and, finally, the associated initiation of the FAZ filament on the cytoplasmic surface of the neck region. A specific microtubule organisation centre must therefore be situated between the basal body and probasal body, and this architecture then defines the microtubules of the quartet as having their plus ends at the anterior of the cell (in contrast to the subpellicular array – the minus ends of which are facing the anterior) (Robinson et al., 1995; Sherwin and Gull, 1989b). Thus, when this quartet subsequently joins the subpellicular array of microtubules, it forms an antiparallel seam along the site of flagellum attachment. Given the number of unusual kinesins in the trypanosome genome (Wickstead and Gull, 2006), it remains an intriguing possibility that this antiparallel seam might act as a specific track for motor proteins directing cellular membrane traffic into or out of the flagellar pocket/basal body area.

Attachment of the microtubule quartet to the cytoplasmic surface of the pocket and neck region membrane presumably provides support to the pocket balloon and rigidity to the extended neck. However, as the quartet is tightly associated to the cytoplasmic surface of these membranes it could also endow particular properties

into that membrane region in comparison with those alongside it. Although we know of a number of microtubule associated proteins (MAPs) in the subpellicular microtubule array (Baines and Gull, 2008; Hertz-Fowler et al., 2001; Vedrenne et al., 2002), there is no evidence for MAPs that locate specifically to the microtubule quartet. Further insight to components may shed light on attachment to the inner surface of the pocket membrane and how variation in the intermicrotubule packing in the pocket and the cell body areas are orchestrated.

The tomographic analysis displayed here allows a much clearer demonstration of the structural organisation of a crucial area of the trypanosome. It demonstrates the structural intricacies of the capacity of the basal body complex to act as a master regulator of morphogenesis in the trypanosome and will aid future molecular, functional and mutant studies.

## Materials and Methods

### Cell culture

*Trypanosoma brucei brucei* procyclic forms (strain 427) were cultured at 28°C in SDM 79 medium supplemented with 10% v/v foetal calf serum.

### Sample preparation for electron microscopy

Cells inside the culture flask were chemically fixed for 10 minutes by the addition of enough 25% (w/v) glutaraldehyde to the growing medium to reach a final aldehyde concentration of 2.5%. Cells were collected by centrifugation, re-fixed in 4% (w/v) formaldehyde, 2% (w/v) glutaraldehyde and 0.1% (w/v) picric acid in 100 mM sodium phosphate buffer (pH 7.0) for 1 hour at room temperature, then post-fixed with 1% (w/v) osmium tetroxide in 100 mM sodium phosphate buffer. Fixed cells were washed several times in double-distilled water, en bloc stained with 1% (w/v) aqueous uranyl acetate for 16 hours at 4°C, dehydrated through an acetone series and embedded in epoxy resin.

### Transmission electron microscopy

Plastic embedded cells were thin-sectioned, post-stained with aqueous uranyl acetate and Reynold's lead citrate, and viewed in an FEI Tecnai-F12 electron microscope operating at 80 KeV. Specimens for negatively stained isolated flagella and scanning electron microscopy were prepared as previously described (Sherwin and Gull, 1989a). Whole-mount cytoskeletons were prepared by settling cells onto formvar, carbon-coated, glow discharged grids; extracting with 1% v/v nonidet P-40 in PEME buffer [0.1 M PIPES, 2 mM EGTA, 1 mM MgSO<sub>4</sub>, 0.1 mM EDTA (pH 6.9)]; fixing in 2.5% (v/v) glutaraldehyde in PEME buffer; and negatively staining with 0.7% (w/v) gold-thiogluconate in water.

### Cellular tomography

Ribbons of serial sections, 250 nm thick, were collected on formvar coated, copper-rhodium slot grids, then post-stained with aqueous uranyl acetate and Reynold's lead citrate. Colloidal gold particles (15 nm) were deposited on both surfaces of the sections for use as fiducial markers during subsequent image alignment. Sections were viewed in an FEI Tecnai-F30 electron microscope operating at 300 KeV, and images recorded digitally with a 2048×2048 pixel CCD camera (Gatan, Pleasanton, CA) using a pixel size of 1.2 nm. Tilt series were recorded with automated methods for image montaging, data acquisition and image alignment as the sample was serially tilted by 1° angular increments over a range of 120° (±60°) about two orthogonal axes with the microscope control program SerialEM (Mastronarde, 2005). 3D distributions of stain density (tomograms) were calculated from each tilt series, aligned with each other and combined to produce a single dual-axis 3D reconstruction (Mastronarde, 1997) measuring 2.4×2.4×0.73 μm<sup>3</sup> (for tomo 1). Tomograms from adjacent sections were aligned to each other, then subcellular structures and membranes within the 3D volumes were analysed and modelled using the IMOD software package (Kremer et al., 1996).

These 3D reconstructions were segmented by modelling features of interest. Experienced investigators used the IMOD package to represent the 3D position, orientation and trajectory of structural components of the flagellar pocket and its surrounding cytoplasmic features: the plasma membrane, the kinetoplast, the flagellum and its associated cytoskeletal components. Each such 3D model was checked and re-evaluated by other investigators until the model represented the complex cytoarchitecture visible in the tomograms to the satisfaction of all concerned. Movie 1 (supplementary material) first shows the 3D tomographic reconstruction, then the tomogram merged with the corresponding model and eventually the 3D model.

Work in K.G.'s laboratory was supported by the Wellcome Trust, Human Frontiers Science Program and the EP Abraham Trust. K.G. is a Wellcome Trust Principal Research Fellow. S.L. is supported by a

Henry Goodger Scholarship. This work benefited from use of electron micrographs collected over many years by previous members of K.G.'s laboratory to whom thanks are due. Electron tomography was carried out in the Boulder Laboratory for 3D Electron Microscopy of Cells, supported by RR000592 from the NIH to J.R.M. Special thanks are due to Boulder colleagues for their expert advice and training. Deposited in PMC for release after 12 months.

## References

- Allen, C. L., Goulding, D. and Field, M. C. (2003). Clathrin-mediated endocytosis is essential in *Trypanosoma brucei*. *EMBO J.* **22**, 4991-5002.
- Atrih, A., Richardson, J. M., Prescott, A. R. and Ferguson, M. A. J. (2005). *Trypanosoma brucei* glycoproteins contain novel giant poly-N-acetyllactosamine carbohydrate chains. *J. Biol. Chem.* **280**, 865-871.
- Baines, A. and Gull, K. (2008). WCB is a C2 domain protein defining the plasma membrane-sub-pellicular microtubule corset of kinetoplastid parasites. *Protist* **159**, 115-125.
- Bangs, J. D., Uyetake, L., Brickman, M. J., Balber, A. E. and Boothroyd, J. C. (1993). Molecular cloning and cellular localisation of a BiP homolog in *Trypanosoma brucei*-divergent ER retention signals in a lower eukaryote. *J. Cell Sci.* **105**, 1101-1113.
- Bastin, P., Pullen, T., Moreira-Leite, F. and Gull, K. (2000). Inside and outside of the trypanosome flagellum: a multifunctional organelle. *Microbes Infect.* **2**, 1865-1874.
- Beattie, P. and Gull, K. (1997). Cytoskeletal architecture and components involved in the attachment of *Trypanosoma congolense* epimastigotes. *Parasitology* **115**, 47-55.
- Bonhivers, M., Nowacki, S., Landrein, N. and Robinson, D. R. (2008). Biogenesis of the trypanosome endo-exocytotic organelle is cytoskeleton mediated. *PLoS Biol.* **6**, e105.
- Briggs, L. J., McKean, P. G., Baines, A., Moreira-Leite, F., Davidge, J., Vaughan, S. and Gull, K. (2004). The flagella connector of *Trypanosoma brucei*: an unusual mobile transmembrane junction. *J. Cell Sci.* **117**, 1641-1651.
- Broadhead, R., Dawe, H. R., Farr, H., Griffiths, S., Hart, S. R., Portman, N., Shaw, M. K., Ginger, M. L., Gaskell, S. J., McKean, P. G. et al. (2006). Flagellar motility is required for the viability of the bloodstream trypanosome. *Nature* **440**, 224-227.
- Chanex, A. L., Hehl, A. B., Engstler, M. and Schneider, A. (2006). Ablation of the single dynamin of *T. brucei* blocks mitochondrial fission and endocytosis and leads to a precise cytokinesis arrest. *J. Cell Sci.* **119**, 2968-2974.
- de Graffenried, C. L., Ho, H. H. and Warren, G. (2008). Polo-like kinase is required for Golgi and bilobe biogenesis in *Trypanosoma brucei*. *J. Cell Biol.* **181**, 431-438.
- Engstler, M., Pfohl, T., Herminghaus, S., Boshart, M., Wiegertjes, G., Heddergott, N. and Overath, P. (2007). Hydrodynamic flow-mediated protein sorting on the cell surface of trypanosomes. *Cell* **131**, 505-515.
- Field, M. C. and Carrington, M. (2004). Intracellular membrane transport systems in *Trypanosoma brucei*. *Traffic* **5**, 905-913.
- Field, M. C., Natesan, S. K. A., Gabernet-Castello, C. and Koumandou, V. L. (2007). Intracellular trafficking in the trypanosomatids. *Traffic* **8**, 629-639.
- Garcia-Salcedo, J. A., Perez-Morga, D., Gijon, P., Dilbeck, V., Pays, E. and Nolan, D. P. (2004). A differential role for actin during the life cycle of *Trypanosoma brucei*. *EMBO J.* **23**, 780-789.
- Geimer, S. and Melkonian, M. (2004). The ultrastructure of the *Chlamydomonas reinhardtii* basal apparatus: identification of an early marker of radial asymmetry inherent in the basal body. *J. Cell Sci.* **117**, 2663-2674.
- Gull, K. (1999). The cytoskeleton of trypanosomatid parasites. *Annu. Rev. Microbiol.* **53**, 629-655.
- Gull, K. (2003). Host-parasite interactions and trypanosome morphogenesis: a flagellar pocketful of goodies. *Curr. Opin. Microbiol.* **6**, 365-370.
- He, C. Y., Ho, H. H., Malsam, H., Chalouni, C., West, C. M., Ullu, E., Toomre, D. and Warren, G. (2004). Golgi duplication in *Trypanosoma brucei*. *J. Cell Biol.* **165**, 313-321.
- He, C. Y., Pypaert, M. and Warren, G. (2005). Golgi duplication in *Trypanosoma brucei* requires Centrin2. *Science* **310**, 1196-1198.
- Henley, G. L., Lee, C. M. and Takeuchi, A. (1978). Electron-microscopic observations on *Trypanosoma brucei* freeze cleaving and thin sectioning study of apical part of flagellar pocket. *Z. Parasitenkd.* **55**, 181-187.
- Hertz-Fowler, C., Ersfeld, K. and Gull, K. (2001). CAP5.5, a life-cycle-regulated, cytoskeleton-associated protein is a member of a novel family of calpain-related proteins in *Trypanosoma brucei*. *Mol. Biol. Parasitol.* **116**, 25-34.
- Hung, C. H., Qiao, X. G., Lee, P. T. and Lee, M. G. S. (2004). Clathrin-dependent targeting of receptors to the flagellar pocket of procyclic-form *Trypanosoma brucei*. *Eukaryotic Cell* **3**, 1004-1014.
- Kremer, J. R., Mastrorarde, D. N. and McIntosh, J. R. (1996). Computer visualization of three-dimensional image data using IMOD. *J. Struct. Biol.* **116**, 71-76.
- Landfear, S. M. and Ignatushchenko, M. (2001). The flagellum and flagellar pocket of trypanosomatids. *Mol. Biochem. Parasitol.* **115**, 1-17.
- Mastrorarde, D. N. (1997). Dual-axis tomography: an approach with alignment methods that preserve resolution. *J. Struct. Biol.* **120**, 343-352.
- Mastrorarde, D. N. (2005). Automated electron microscope tomography using robust prediction of specimen movements. *J. Struct. Biol.* **152**, 36-51.
- Moestrup, O. (2000). The flagellate cytoskeleton: introduction of a general terminology for microtubular flagellar roots in protists. In *The Flagellates: Unity, Diversity and Evolution* (ed. B. S. C. Leadbetter and J. C. Green). New York: Taylor and Francis.
- Moreira-Leite, F. F., Sherwin, T., Kohl, L. and Gull, K. (2001). A trypanosome structure involved in transmitting cytoplasmic information during cell division. *Science* **294**, 610-612.
- O'Toole, E. T., Giddings, T. H., McIntosh, J. R. and Dutcher, S. K. (2003). Three-dimensional organization of basal bodies from wild-type and delta-tubulin deletion strains of *Chlamydomonas reinhardtii*. *Mol. Biol. Cell* **14**, 2999-3012.
- Oberholzer, M., Bregy, P., Marti, G., Minca, M., Peier, M. and Seebeck, T. (2007a). Trypanosomes and mammalian sperm: one of a kind? *Trends Parasitol.* **23**, 71-77.
- Oberholzer, M., Marti, G., Baresic, M., Kunz, S., Hemphill, A. and Seebeck, T. (2007b). The *Trypanosoma brucei* cAMP phosphodiesterases TbrPDEB1 and TbrPDEB2: flagellar enzymes that are essential for parasite virulence. *FASEB J.* **21**, 720-731.
- Ogbadoyi, E. O., Robinson, D. R. and Gull, K. (2003). A high-order trans-membrane structural linkage is responsible for mitochondrial genome positioning and segregation by flagellar basal bodies in trypanosomes. *Mol. Biol. Cell* **14**, 1769-1779.
- Overath, P. and Engstler, M. (2004). Endocytosis, membrane recycling and sorting of GPI-anchored proteins: *Trypanosoma brucei* as a model system. *Mol. Microbiol.* **53**, 735-744.
- Pays, E., Vanhollenbeke, B., Vanhamme, L., Paturiaux-Hanocq, F., Nolan, D. P. and Perez-Morga, D. (2006). The trypanolytic factor of human serum. *Nat. Rev. Microbiol.* **4**, 477-486.
- Ploubidou, A., Robinson, D. R., Docherty, R. C., Ogbadoyi, E. O. and Gull, K. (1999). Evidence for novel cell cycle checkpoints in trypanosomes: kinetoplast segregation and cytokinesis in the absence of mitosis. *J. Cell Sci.* **112**, 4641-4650.
- Robinson, D. R. and Gull, K. (1991). Basal body movements as a mechanism for mitochondrial genome segregation in the trypanosome cell cycle. *Nature* **352**, 731-733.
- Robinson, D. R., Sherwin, T., Ploubidou, A., Byard, E. H. and Gull, K. (1995). Microtubule polarity and dynamics in the control of organelle positioning, segregation, and cytokinesis in the trypanosome cell cycle. *J. Cell Biol.* **128**, 1163-1172.
- Rosenbaum, J. L. and Witman, G. B. (2002). Intraflagellar transport. *Nat. Rev. Mol. Cell Biol.* **3**, 813-825.
- Schwartz, K. J., Peck, R. F., Tazeh, N. N. and Bangs, J. D. (2005). GPI valence and the fate of secretory membrane proteins in African trypanosomes. *J. Cell Sci.* **118**, 5499-5511.
- Sherwin, T. and Gull, K. (1989a). The cell division cycle of *Trypanosoma brucei brucei*-timing of event markers and cytoskeletal modulations. *Philos. Trans. R. Soc. Lond. B Biol. Sci.* **323**, 573-588.
- Sherwin, T. and Gull, K. (1989b). Visualization of deetyrosination along single microtubules reveals novel mechanisms of assembly during cytoskeletal duplication in trypanosomes. *Cell* **57**, 211-221.
- Shiflett, A. M., Faulkner, S. D., Cotlin, L. F., Widener, J., Stephens, N. and Hajduk, S. L. (2007). African trypanosomes: intracellular trafficking of host defense molecules. *J. Eukaryot. Microbiol.* **54**, 18-21.
- Stephan, A., Vaughan, S., Shaw, M. K., Gull, K. and McKean, P. G. (2007). An essential quality control mechanism at the eukaryotic basal body prior to intraflagellar transport. *Traffic* **8**, 1323-1330.
- Steverding, D. (2000). The transferrin receptor of *Trypanosoma brucei*. *Parasitol. Int.* **48**, 191-198.
- Taylor, A. E. R. and Godfrey, D. G. (1969). A new organelle of bloodstream salivarian trypanosomes. *J. Protozool.* **16**, 466-470.
- Vanhollenbeke, B., De Muylder, G., Nielsen, M. J., Pays, A., Tebabi, P., Dieu, M., Raes, M., Moestrup, S. K. and Pays, E. (2008). A haptoglobin-hemoglobin receptor conveys innate immunity to *Trypanosoma brucei* in humans. *Science* **320**, 677-681.
- Vaughan, S., Kohl, L., Ngai, L., Wheeler, R. J. and Gull, K. (2008). A repetitive protein essential for the flagellum attachment zone filament structure and function in *Trypanosoma brucei*. *Protist* **159**, 127-136.
- Vedrenne, C., Giroud, C., Robinson, D. R., Besteiro, S. B., Bosc, C., Bringaud, F. and Baltz, T. (2002). Two related subpellicular cytoskeleton-associated proteins in *Trypanosoma brucei* stabilize microtubules. *Mol. Biol. Cell* **13**, 1058-1070.
- Vickerman, K. (1973). Mode of attachment of *Trypanosoma vivax* in proboscis of tsetse fly *Glossina fuscipes*-ultrastructural study of epimastigote stage of trypanosome. *J. Protozool.* **20**, 394-404.
- Vickerman, K. and Tetley, L. (1990). Flagellar surfaces of parasitic protozoa and their role in attachment. In *Ciliary and Flagellar Membranes* (ed. R. A. Bloodgood), pp. 267-303. New York: Plenum Press.
- Wickstead, B. and Gull, K. (2006). A "holistic" kinesin phylogeny reveals new kinesin families and predicts protein functions. *Mol. Biol. Cell* **17**, 1734-1743.